Revision Submitted to *Planetary and Space Physics*
Special Section on Proceedings from the
AGU Chapman conference on *Magnetospheric ULF Waves*

Ground Pc3-Pc5 Wave Power Distribution and Response to Solar Wind Velocity Time Variations

D. Vassiliadis[1]

I.R. Mann[2]

S.F. Fung[3]

X. Shao[4]

[1] ST at Code 612.2, NASA/Goddard Space Flight Center
[2] Department of Physics, University of Alberta
[3] Code 612.4, NASA/Goddard Space Flight Center
[4] NRC at Code 612.4, NASA/Goddard Space Flight Center

Abstract.

We examine the wave power in the Pc3-Pc5 range in terms of its growth and decay characteristics and its distribution in L shell in response to an important interplanetary driver, the plasma velocity, V_{SW}. We use nonlinear correlation and filtering methods to quantify the strong coupling of the wave power to V_{SW} variations. Our database includes two years of solar maximum data (2002-2003) of measurements from 26 magnetometers of the IMAGE array and NOAA's GOES-10 spacecraft at geosynchronous orbit. We find that the ground ULF wave power is structured in the range $3.5<L<6.4$ and distributed approximately uniformly in the range $6.4<L<15$ (uncertainties are estimated to be ± 0.5). The response of the wave power to the V_{SW} is characterized by an increase starting 3 days before the V_{SW} peak, intensifying several hours before the peak, followed by a much faster decrease in the next 2 days. The rapid decay of ULF waves, which starts 6 ± 2 hours before the solar wind velocity reaches its peak, is brought about by wave-particle interaction with inner-magnetospheric populations and a dV_{SW}/dt effect. The correlation results are confirmed by calculating the finite-impulse response, which shows clearly the decay of the ULF waves after the V_{SW} peak. The response of the wave power at geosynchronous orbit is very similar to that of the ground wave power at comparable L shells. Effects of the non-Gaussian wave power probability density function on these results are mitigated by the use of rank-order analyses. The results demonstrate several complexities of the wave power response to interplanetary disturbances.

1. Introduction.

The role of ultra-low-frequency (ULF) waves as an important link in the energy and momentum chain that leads from interplanetary space to planetary plasmas has long been known [Engebretson et al., 1994], but is currently being reevaluated. In ground magnetometer arrays we have excellent observatories of the excitation, growth, and damping of waves produced by magnetospheric and ionospheric processes, which are in turn energized by the solar wind-magnetosphere interaction. Using measurements from a meridional array we measure the distribution of solar wind-driven wave power in the range Pc3 to Pc5 (10 sec to 10 min) using correlation techniques. Going beyond correlation analysis, we also measure the response to solar wind velocity using correlations as well as FIR models. The main motivation for characterizing the growth and decay, spatial extent, and other characteristics for the Pc3-Pc5 wave power is the significance of the waves in the acceleration of radiation-belt electrons, especially during magnetic storms. In the remainder of this section we review the excitation and absorption properties of the waves as well as their observed correlation with interplanetary and radiation-belt activity.

Wave excitation and propagation in the magnetosphere.

Low-frequency waves are produced in the magnetosphere both by external (interplanetary) and internal (magnetospheric) effects [Wright and Rickard, 1995; Mann et al., 1999]. The interplanetary effects involve the passage of solar wind structures through geospace and the transfer of energy, momentum, and plasma, while magnetospheric effects involve the redistribution of magnetospheric plasma and energetic particles during storms and substorms. One of the most important external mechanisms is the compression of the magnetosphere by increased solar wind pressure as it occurs during the passage of interplanetary shocks, CMEs, and other solar wind structures [Gonzalez, 1999]. Pressure pulses launch low-frequency waves at the magnetopause, which propagate inward and are amplified in the magnetospheric waveguide [Mann et al., 1999]. In the storm timescales that we are interested in (hours and days), pressure increases due to CMEs and similar structures are important, while those due to shocks are normally too short in duration. A second important interplanetary excitation is via Kelvin-Helmholtz, Rayleigh-Taylor, and other fluid instabilities that occur at the flanks of the magnetosphere as a result of viscous (hydrodynamic) interaction with the solar wind. These effects are observed most clearly when the IMF B_z is Northward [Farrugia et al., 2001], because magnetic reconnection effects are too weak to overwhelm the cold plasma dynamics. Prolonged intervals of increased solar wind velocity are well correlated with ULF wave activity [Mann et al., 2004], especially during high-speed stream (HSS) passages and even more so at solar minimum [Engebretson et al., 1998; Posch et al., 2003]. On average, the correlation between solar wind velocity

and wave power is moderately high, for instance the rank-order correlation coefficient exceeds 60% for data spanning a complete solar cycle (1990-2001) [Mann et al., 2004]. Third, stormtime Pc5 (and other) waves are excited by the dipolarization of nightside field lines following reconnection in the tail [Anderson et al., 1990]. Stormtime activity of the ring current can also excite ULF waves [Thorne and Horne, 1994]. All these and other mechanisms depend on the time history of the solar wind and IMF and the recent state of the magnetosphere (preconditioning).

In the magnetosphere, ULF waves refract and interfere as they propagate. Their 3-dimensional distribution was the focus of several studies [Anderson et al., 1990; Takahashi et al., 2004]. They may form standing waves whose spatial patterns are of importance for particle acceleration. The persistence of Pc5 waves in the magnetosphere depends significantly on the ionospheric state, in particular on the conductivity, which determines the wave power dissipation rate.

Wave interaction with trapped particles.

In the inner magnetosphere, particle acceleration as the interaction with a wave can be expressed in terms of an increase in kinetic energy. We have in mind electron acceleration here, but effects on energetic protons are analogous. The effectiveness of an acceleration process depends on the wave spectral power distribution and overall magnitude, the ratio between the dominant wave timescales and those of the electron adiabatic invariants, etc. Drift resonance of the particle with a monochromatic wave can lead to phase space diffusion [Hudson et al., 1999; Elkington et al., 1999]. The presence of several monochromatic waves at nearby frequencies causes a resonance overlap and the formation of a complex web in phase space connecting low-energy regions to high-energy ones. More typically the electron interacts with a continuous spectrum of waves leading to stochastic acceleration [Liu et al., 1999]. Thus the magnitude and distribution of wave power is a major focal point of this paper.

The close relation between variations in magnetic field, predominantly in the ULF and VLF range, and particle flux levels have been well known [Lanzerotti et al., 1971]. A recent representative paper discussed a comparison of Pc5 wave power with geosynchronous electrons [Rostoker et al., 1998]. They analyzed the wave power in the Pc5 range measured at the Gillam station of the CANOPUS array (CGM Lat.=66.46, L=6.27) and found enhanced activity in the dawn-noon sector over a long interval (95 days) in 1994. The ULF waves were excited by high-speed streams in the solar wind, which are particularly well defined and periodic (at 13.5 and sometimes at 6.25 days) during solar minimum. The clearest evidence for ULF wave power correlations was seen at the edge of the trapped-particle region, close to the geosynchronous orbit at L=6.6, whereas effects in the “heart” of the outer belt (L~4-5) were less intense. Flux measurements were taken at low altitudes by the polar-orbiting SAMPEX spacecraft and compared to those at the equatorial plane taken by GOES-7.

While most earlier studies are limited to one or a few locations for the measurement of the wave power, it is clear that the spatial structure of the wave power is of significance because it modulates the energy transfer and can be used to identify the type of acceleration.

A second focus is the response of the wave fields to disturbances in the solar wind or IMF, especially those variables that are important in determining the dynamics of the energetic electron flux [Vassiliadis et al., 2002; 2003; 2005].

A three-way comparison between solar wind speed, ULF wave power and energetic electron fluxes was made recently [Mann et al., 2004]. In addition to the moderately strong correlations between solar wind speed and all three **B**-field components measured at two different ground stations, the study reported high correlations between the ground wave power and the flux measured at L=4.5 and 5.5 by HEO spacecraft 1994-2026 and at geosynchronous obit by Los Alamos National Laboratory satellites.

In the following sections we examine the effects of solar wind velocity variations on the ULF wave power from several different new perspectives. We use time series data of the wave power on the ground parameterized by L shell, $P_{ULF}(t;L)$, from a dense high-latitude meridional array, and compare the findings to those obtained from GOES-10 observations at geosynchronous orbit (Section 2). We also use traditional correlative analysis and complement it with rank-order correlation functions to mitigate possible effects of the power data distribution on the techniques (Section 3). While correlative analysis is useful for understanding the basic effects, we also develop a basic linear model (Section 4). The model demonstrates the average profile of the wave power following an increase in solar wind velocity and provides more detailed information about the interaction than the correlation function.

2. Observations

We have compiled a database of ground-magnetometer measurements of ULF wave fields in the Pc3-Pc5 range in 2002-2003, and included simultaneous GOES-10 observations of the wave magnetic field at the geosynchronous orbit. The observation interval has been chosen because of the intense and significant heliospheric and magnetic-storm activity during the most recent solar maximum. We have compared the time variations of the wave power on the ground and at geosynchronous orbit with several IMF and solar wind parameters measured upstream of Earth, obtained from the OMNI database of NASA's NSSDC.

Measurements of the ground field were taken at the 27 magnetometers of the IMAGE array, an international scientific collaboration managed by the Finnish Meteorological Institute. The magnetometers span the range of 54.5°-75.3° in corrected geomagnetic latitude and 3.0-15.4 in L shell, both calculated with the GEO-CGM code [Gustafsson et al., 1992]. For L>12, uncertainties in the value of L increase rapidly, which affects statements about 3 stations (HOR, LYR, NAL). Note, however, that the wave power at these stations is well correlated with each other as well as with the power at the immediately more equatorial stations to about L=6.36.

The spectral energy decreases with frequency (roughly as a power law with spectral index –0.5) and we high-pass filter the 10-sec-resolution magnetic field data with an MA filter of Δt=10 min. Daily averages of the ground wave power, $P_{ULF}(t;L)$, time series at fixed L are shown for the year 2003 in Fig. 1. The large excursions at DOY 300-304 are wave power increases during the so-called "Halloween storms" at the end of October 2003. In the two years we have analyzed (2002-2003) missing data are less than 10% for 20 of the IMAGE magnetometers and less than 20% for 4 more instruments. One magnetometer in the Southern part of IMAGE had more than 20% data gaps and was not used.

The ground wave power at L~6.6 was compared to that obtained from GOES-10 measurements. Gaps in the original GOES-10 minute averages are of the order of 1%.

The wave activity is correlated with several interplanetary parameters, primarily the solar wind velocity, V_{SW}. Fig. 2 shows hourly averages of the wave power measured at Tromso at L=6.36 (top) and the solar wind velocity (bottom). The autocorrelation of the wave power time series is 12±4 hours while that of V_{SW} are 6±1 days. Although the variations of the time series are qualitatively different, the ULF wave activity has been linked to the solar wind velocity variations [Engebretson et al., 1998], and we will further describe their relation in this paper.

Certain properties of the sample probability density function (pdf) of these variables are important in the analysis to follow. Specifically, the pdf's of the wave power, and to a lesser extend of the solar wind velocity, are markedly non-Gaussian and have a significant skewness. The estimation of statistical and probability measures may therefore be biased by the relatively few large-amplitude events. We use two different methods to eliminate such a possible bias due to the data distribution: we first use the square root of the ULF wave power, $P_{ULF}^{1/2}$, as the primary variable. The square root has a much less skewed and more stationary pdf than the original wave power. Second, we calculate the rank-orderings of both the wave power and the solar wind velocity and apply the same correlative and

filter techniques to them as we do with the raw data. Using the rank orderings is a standard way of ensuring statistically robust analysis. We then compare results from the two approaches.

3. Excitation of Pc3-Pc5 Waves by the Solar wind Speed: Correlation analysis

ULF wave growth has been linked to several interplanetary and magnetospheric parameters as already discussed in Section 1. In particular, there is an observed relation between the wave power P_{ULF} and solar wind velocity V_{SW} (Fig. 2), which corresponds to a basic time-independent model representing hydrodynamic changes such as compressions of the magnetosphere or viscous interaction with the solar wind. When a change in V_{SW} is made, the wave power starts to change after a time $\tau = \tau_{SW} + \tau_g + \tau_{MS}$, where τ_{SW} is the solar wind propagation time from an upstream measurement point to the subsolar magnetospheric region in the magnetosheath; τ_g is the growth time of waves close to and inside of the magnetopause boundary; and τ_{MS} is the time for wave propagation from the magnetopause to the point of measurement in the magnetosphere. In actuality waves are transmitted across the entire dayside magnetopause and not only the subsolar point, so τ_{SW} is a lower bound; also waves can grow as they propagate in the magnetosphere so the total time inside the magnetosphere generally differs from the sum $\tau_g+\tau_{MS}$.

The delay in increase of the wave power relative to the solar wind velocity is estimated from the correlation function:

$$C_{P_{ULF}^{1/2},V_{SW}}(\tau) = \frac{1}{T}\frac{1}{\sigma_{P_w}\sigma_{V_{SW}}}\int_0^T \left(P_{ULF}^{1/2}(t+\tau) - \overline{P_{ULF}^{1/2}}\right)\left(V_{SW}(t) - \overline{V}_{SW}\right)dt \qquad (1)$$

where T is the length of the time series, $\overline{P_{ULF}^{1/2}}$ and $\overline{V}_{SW}$ denote time series averages, and σ_{P_w} and $\sigma_{V_{SW}}$ the corresponding standard deviations. The lag τ=0 represents the time of occurrence of the V_{SW} peak and finite lag values indicate the ULF wave response relative to that peak.

In Fig. 3 we compare three correlation functions, two based on ULF wave power measured by ground stations and one from the geosynchronous orbit. The Oulujaervi (OUJ) station is at corrected magnetic latitude MLAT=66.6 and, under quiet conditions, it maps close to the "heart" of the outer electron radiation belt (L=4.25). Similarly, Tromso (TRO) is at MLAT=66.6 with L=6.36, close to the edge of the outer belt. The GOES-10 spacecraft is at geosynchronous orbit and we will represent its L shell as 6.6 although in reality its L varies depending on solar wind pressure and IMF orientation. There is a strong similarity between the three functions, esp. between TRO and GOES-10. All three functions reach their maximum at $\tau \le 0$, following by a rapid decline for τ>0. The maximum value of

(1) is 66.6% at OUJ, 44% at TRO, and 40% at GEO. Thus the historical time variations of the solar wind velocity explain approximately the square of the correlation, viz. 44% of the variance of the historical $P_w^{(g)}$ time series from Oulujaervi and 16-20% of the variance of the power at the other two locations. There is a secondary, shallower minimum at ~13 ½ days after the first one, owing to the sector organization of the solar wind producing a quasiperiodic component in V_{SW}.

Rank-order correlation function.

We also compute the rank-order correlation function, which is analogous to (1) and generalizes the rank-order correlation coefficient [Press et al., 1992; Mann et al., 2004]. The rank-order correlation function is a more robust estimator for analysis of nonstationary time series data than the regular correlation function, which can be biased by the largest events in the sample. The rank-order correlations for the three individual magnetometer platforms, TRO, OUJ, and GOES-10, are very similar to those shown in Fig. 3, but are generally higher in amplitude.

It is important to accurately establish the location of the peak of the correlation functions: a peak at $\tau=0$ indicates that the ULF wave excitation involves a "dV_{SW}/dt" effect where an increasing velocity drives wave excitation processes and a decreasing velocity damps them down; a peak at $\tau<0$ indicates a different mechanism, for instance waves are produced when the velocity exceeds a threshold value as it rises towards its peak, etc. Using hourly data we find that the rank-order correlation function peaks are at τ=-6 h and –8 h for OUJ and TRO, resp., and at –15 h for wave power measured by GOES-10, as evidenced in Fig. 4. In fact for most ground stations, the peak occurs at $-8 \le \tau \le -6$ (stations at L=3.5-4 have delays of 4-5 hours). The peak location does not support a dV_{SW}/dt effect for the ULF wave excitation, but suggests other possible mechanisms. One caveat is that this approach does not account for an MLT variation in wave power in this paper. Proper study of the MLT dependence of the response will require comparison between simultaneous measurements from two or more longitudinally distributed stations and will be pursued in a future work.

Correlation at $\tau<0$: what about causality?

The correlation at negative lags is high and prolonged indicating that the interaction takes place over several days before the peak of the solar wind. For several ground stations as well as GOES-10, the peak occurs at τ~-1 day for both the regular and the rank correlation, and there is significant correlation for at least 1 additional day prior. Since the correlation (1) is computed in reference to the solar wind velocity, a correlation peak at positive (negative) lags means that the wave power is correlated with earlier (later) solar wind velocities. At first sight therefore the negative-lag correlation appears acausal. By taking into account, however, that the solar wind velocity varies more slowly than

the wave power (Fig. 2), what the negative-τ peak actually means is that in most cases, the maximum wave power occurs before the peak solar wind velocity.

A discussion of the correlation at $\tau<0$ was presented by Engebretson et al. [1998] who plotted the daily Pc5 wave power versus the daily V_{SW} during intervals of highly periodic high-speed stream activity in solar minimum (1993): they found that the power rises during the ascending part of the stream, but rapidly decays before the long-lasting stream reaches its peak velocity.

In our case, the epoch is 2003 (post-solar maximum) and the dataset includes both high-speed streams as well as significant CME-driven activity. For CMEs we expect the correlation peak to occur at $\tau=0$ or later, since the solar wind changes abruptly, in the order of even a few minutes and it produces high ULF wave power at the onset of activity. To verify this expectation, we repeated the m rank correlation analysis with subsets of the hourly data comprising solely CME-type or HSS-type intervals. The CME intervals were identified in terms of high speed, density, and magnetic field as follows: $V_{SW} > 700$ km/sec, $n_{SW} > 2$ cm^{-3}; $|B|>1$ nT. The sample included 622 hourly averages or 3.6% of the two-year dataset. The peak of the rank correlation was at $\tau_{peak}=0\pm2$ hours for most stations. HSS intervals were identified in terms of comparably high speed as the CMEs, low density and no dependence on the magnetic field as follows: $V_{SW} > 700$ km/sec and $n_{SW} < 2$ cm^{-3}. This sample included 595 hourly averages or 3.4% of the original dataset. The rank correlation peak was at $\tau=1$-11 ± 4 hours, much closer to the peak locations described above. Thus while CMEs do produce a different response in the ULF wave power, statistically their occurrence is much lower than that of high-speed streams. An earlier study using daily average data showed that the rank-correlation peak does not vary significantly with solar cycle phase [Mann et al., 2004].

Correlation at $\tau\geq0$: wave damping.

The rapidly declining correlation at $\tau\geq-4$ hours (for most stations) is an indication that wave power decays at a time-varying rate. The correlation decreases slowly until $\tau=0$ and then much more rapidly. For several ground stations as well as GOES-10, the derivative of the correlation function decreases discontinuously at $\tau=0$, indicating two different damping effects (see for example the GOES-10 line in Fig. 4). Wave damping can be produced by a dV_{SW}/dt driver (which is turned off at $\tau=0$) as well as a change in the damping parameters such as a change in the particle population in resonance with the waves. The net result is that the wave power is absorbed at a rate which overcomes any excitatory effects due to V_{SW} (which may still be increasing especially for long, slow-moving clouds and CMEs).

The rate of decrease becomes faster at $\tau>0$, and for most ground stations the correlation function is concave at those lags:

$$\frac{d^2 C_{P_{ULF}^{1/2}, V_{SW}}}{dt^2} > 0, \quad \tau > 0 \qquad (2)$$

while typical correlation functions are convex on either side of their maximum. The difference between the two rates of decrease indicates that there are more than one processes leading to the decrease of the ULF wav power.

In summary there are several indications that (at least) two different processes contribute to wave damping, one after the peak and one after τ=0.

Latitudinal distribution of the wave power.

We interpolate in L the rank-order correlation functions from individual ground magnetometers to obtain a two-dimensional correlation function C=C(τ,L). The function is shown in Fig. 5 for each of the two years considered; qualitatively it is the same for both years. The main peak occurs at $-3 < \tau \leq 0$ for almost all L shells. The correlation is a smooth function of L for L>6.36, but becomes rough and noisy in the intermediate L range 4<L<6.36. Uncertainties in L for those boundaries are estimated at ±0.5 for this long dataset; at shorter timescales (spanning one or several storms) the location of these boundaries varies significantly. Below L=3.5 wave power varies again smoothly as a function of L. The contrast between a highly structured correlation in the region 4<L<6.36 and smooth correlations in the two regions at higher and lower L shells is much more pronounced when we use hourly averages than daily data.

ULF waves have a complex mode structure, which is a function of L shell, polarization, and activity level [Anderson et al., 1990]. The structure of the ULF waves seen on the ground is also determined by convection and induced ionospheric currents, especially at auroral latitudes. The complex mode structure determines the impact of the waves on accelerating particles [Hudson et al., 1998]. The complex mode structure is manifested here in the nonuniform structure of the rank-order correlation as a function of L in the intermediate L range (4-6.36).

Therefore it is important to use a large number of magnetometers to sample the wave power structure at 4<L<6.36, but only a few at lower and higher L shells. Earlier studies used small numbers of magnetometers and therefore could not determine the difference between the different regions [Engebretson et al., 1998; Mann et al., 2004].

4. The Finite-Impulse-Response Model

The correlation function (1) implies that the wave power has a unique, time-independent delay relative to the solar wind velocity which is not well satisfied: the correlation peaks have a width of

several days (Fig. 3). We therefore introduce a more general model. The correlation function can be obtained from the model, but not vice versa. The model shows the average time development of the wave power at the time of a solar wind intensification in more detail than correlative methods.

Impulse response functions.

The wave power at a specific time is probably due to several velocity disturbances from a number of earlier instances in the past, with varying excitation and transmission efficiencies. Said otherwise, the effects of a disturbance in V_{SW} generally last for more than one day. We represent the relation between V_{SW} and power $P_{ULF}(\mathbf{x};t)$ at position **x** (in geospace or on the ground) using the Finite Impulse Response (FIR) model:

$$P_{ULF}^{1/2}(t;\mathbf{x}_s) = \int_{-T_s}^{T_e} H_{V_{SW}}^{P_{ULF}^{1/2}}(\tau;\mathbf{x}_s) V_{SW}(t-\tau)\, d\tau \qquad (3)$$

The impulse response function (IRF) $H_{V_{SW}}^{P_{ULF}^{1/2}}(\tau;\mathbf{x})$ is a function of time lag τ and parameterized by position **x**. The IRF has a finite duration (from $\tau=-T_s$ to $\tau=T_e$), hence the model name. The function contains all the information related to linear, time-invariant dynamics of the wave power, and can be generalized to nonlinear dynamics. FIR models have been successfully used in modeling the time variations of magnetic indices [Iyemori et al., 1979; Clauer, 1986; Bargatze et al. 1985], those of the high-latitude magnetic-field [Vassiliadis et al., 2002a], and of the radiation-belt electron flux [Vassiliadis et al., 2002; Rigler et al., 2004].

The resulting IRFs (3) are highly unusual in form, in a way even more striking than that in the case of the correlation function. Representative IRFs for the wave power at TRO, OUJ, and GOES-10, computed from the two-year dataset, are shown in Fig. 6. We have used T_s=10 d and T_c=20 d, timescales comparable to storm growth and decay scales, as well as the timing of recurring solar disturbances. The two ground-based IRFs are fairly similar in phase, but differ in peak amplitude. For the Tromso data, the response has a minimum at τ=-3 d, turns positive at τ=-2 days and reaches its peak at day 0. It becomes negative the following day, τ=1, and oscillates towards zero in the next 2 days. If the peak amplitude of H(τ;L) is 0.05 $nT/(km/\sec)$, a solar wind velocity of 600 km/sec lasting 3 days will result in a wave amplitude of ~7.2 nT. The IRF of the GOES-10 wave power has a smaller amplitude due to the lower wave power at the geosynchronous region, but otherwise has a remarkably similar phase variation to the two ground-based responses.

These features are small in amplitude, but are statistically significant because they occur for many of the 26 stations we have examined, and are particularly similar for nearby stations. Uncertainties in

the IRF coefficients are calculated from the SVD solution of the linear equations (3) [Press et al., 1992].

The two unusual features of these IRFs are: a) the peak IRF occurs at $\tau \leq 0$ meaning, again, that the waves are excited well before V_{SW} reaches its highest amplitude. The duration of the solar wind speed input which produces Pc3-Pc5 waves is >3 days such as in the cases of a high-speed stream or a slow-moving CME or magnetic cloud; b) the response decays rapidly at $\tau>0$ and, rather than going to zero, it has one or more negative peaks, the most prominent at τ = 1 day. At several ground stations, the response is oscillatory for more than 3 days before it reaches zero. IRFs based on hourly data have been computed and confirm the results based on daily averaged data. They will be presented in a different study.

Rank-order impulse response functions.

In order to mitigate any effects due to the data distribution we have defined and calculated a rank-order impulse response function in a way analogous to Eq. (3). Rank responses are shown in Fig. 7 for wave data from the same three platforms as in the previous figure. In addition to τ=0 peak, the three waveforms have several elements in common: the increase at τ=-2 d, a rapid decrease at τ=1 d, and a recovery at τ=2-3 d. Even features at longer lags are in good agreement. In the following we discuss regular and rank-order IRFs together, distinguishing them where needed.

Response at $\tau>0$: wave damping.

The negative peak at τ=1 d represents the rapid absorption of the waves soon after their growth. The peak may be due to the V_{SW}-driving being turned off (the dV_{SW}/dt effect), but it may also be due to additional internal magnetospheric effects. By "internal" we mean magnetospheric effects not directly linked to the solar wind state, such as those arising from storage and unloading. A first piece of evidence of this effect includes instances when the wave power decreases while V_{SW} is still rising as shown in Fig. 2 and as discussed for recurrent HSSs by Engebretson et al. [1998]. A second indication is the two-slope decay of the correlation, one for $\tau<0$ and one for $\tau>0$.

In view of this evidence, the negative peak is not a solar wind velocity effect, but appears because the wave power time series contain characteristic rapid decay patterns (Fig. 2) due to a physical mechanism distinct from those driven by V_{SW}. This is a common occurrence in systems driven with multiple inputs, where not all of these inputs are observed: some IRF peaks represent effects due to the observed inputs while other represent effects due to the unobserved ones because these effects are contained in the observed output.

Therefore, while the positive peak of the IRF is consistent with wave excitation by V_{SW}-driven processes, the negative peak cannot be explained by the variations of the solar wind velocity alone. The velocity can contribute to the decay of the ULF wave power through a dV_{SW}/dt-type effect.

However, the fact that the rank-correlation peak occurs at negative lags shows that there are additional magnetospheric effects added to those of V_{SW}. The magnetospheric effects that contribute to the wave damping are probably due to the stormtime enhancement of those particle populations that interact with the waves. In the discussion section we discuss the role of several types of particle populations with the ULF wave fields.

Latitudinal distribution.

We interpolate in L the rank-order IRFs to obtain a synoptic view of the response as a function of time lag and L (Fig. 8). On the left side of the image, diamonds indicate the locations of the IMAGE magnetometers. Evidently, the response peaks discussed above are actually representative of a broad range of L shells. Both peak amplitudes and lags are similar in L=3.5-8.5 with the peak amplitude occurring in L=4.61 at the Rorvik (RVK) station (Fig. 9a).

Model performance.

The FIR model developed for each L shell explains a percentage of the time variations of the recorded wave power. The capability of the model to reproduce the observed time variations is measured as the data-model correlation coefficient between observations and model output (Fig. 9b). The region 4<L<6.6 has a somewhat higher correlation of ~50% compared to L>6.6. The model from the GOES-10 data has a somewhat lower correlation of 47.2%. The prediction efficiency (percent variance explained by the FIR model) is approximately the square of the data-model correlation coefficient.

5. Discussion

The relation between time variations of the solar wind velocity and those of the ULF wave power in the Pc3-Pc5 range is a complex one. A number of contributing mechanisms, the dependence on the global magnetospheric activity and large-scale configuration, and boundary effects, add to the complexity. It is clear, however, that increases in V_{SW}, such as those during high-speed streams, CMEs, and even shocks, result in a global intensification of ULF wave power in the magnetosphere and on the ground.

We reported on the timing, spatial distribution, and coupling strength of the effective interaction between V_{SW} and P_{ULF} as observed from geosynchronous orbit and from the ground. Regarding the timing, the correlation and FIR analysis demonstrate that wave power becomes significant soon after the solar wind velocity starts increasing (peak at τ=0), but starts declining several hours before V_{SW}

reaches its peak (positive correlation and impulse response at $\tau<0$). The interpretation is that processes unrelated to the velocity, such as wave-particle interactions, lead to (non)resonant absorption of the waves.

The correlation analysis results are consistent with the findings of Engebretson et al. [1998] who noted this feature examining daily-averaged wave-power measurements for the effect of two recurrent high-speed streams on two high-latitude stations in the last six months of 1993. (One of the stations, Kevo (KEV), belongs to the IMAGE array and was included in the analysis presented above.) Engebretson et al. [1998] found that the wave power was strongest in the leading edge of the stream and subsided more quickly than the solar wind velocity producing it. In our case, the epoch is 2003 (post-solar maximum) which includes both high-speed streams as well as some CME-driven activity. However, we saw that the presence of the CMEs does not make a statistically significant difference in the results obtained from the entire dataset. The study of Mann et al. [2004] showed that the peak correlation does not change significantly as a function of solar cycle phase.

We have further shown that the wave excitation occurs in a broad region in L shell, $L>4.25$, but its amplitude varies as a function of L. In the region $4.25<L<6.36$, there are significant differences between P_{ULF} time series even from nearby stations (where "nearby" is of the order of 100 km). As Figs. 5 and 8 suggest, both the correlation and the impulse response have a structured (noisy) L profile in that region. In contrast to the intermediate region, at higher latitudes, $6.36<L<15$ the wave power appears to vary smoothly with L. The difference between the two regions is due to the spatial structure of the wave field at intermediate L shells (4-6.36) and electrodynamic effects (presence of electrojets and related currents) at higher L shells. A large number of stations is needed to adequately observe ULF variations at the intermediate L shells while a smaller number of stations seems sufficient at $L>6.36$. At low L shells (3.5-4) the wave power is small and uncorrelated with the solar wind velocity, except at stormtime intervals when there is a penetration of ULF power at those latitudes.

The correlation and impulse response functions show that the wave power increases soon after the solar wind velocity starts increasing, but starts declining before V_{SW} reaches its peak. The correlation peak occurs 4-8 hours before $\tau=0$ for stations with $L \geq 4.25$. The finite-τ correlation peak as well as examination of the time series provide evidence for a response beyond the dV_{SW}/dt effect. The decrease of the correlation and impulse responses are most probably due to a wave absorption process rather than a decline in solar wind velocity. As shown in several ways in this paper and in the [Engebretson et al., 1998] scatter plots***, the wave damping is sufficiently strong that it overcomes any additional excitation of waves due to the still growing solar wind velocity.

Thus there is only a narrow time window for ULF waves to be important in particle acceleration, especially compared to the timescales of the velocity changes that are one of their main drivers. As

discussed in Section 2, the timescales of the wave power variation are of the order of 1 day or less whereas V_{SW} varies over several days (CMEs, magnetic clouds) or longer (sector structure).

The origin of the wave damping is probably related to particle acceleration and/or heating. Three possible candidates are energetic electrons in the radiation belts, cold electrons in the plasmasphere, and ring current ions; all three vary significantly during magnetic storms and some of these variations are expected to be linked to the intensification of Pc3-Pc5 waves. We briefly discuss each one next.

While energetic electrons are an obvious recipient of ULF wave power, their flux may not be sufficiently high to account for the entire dissipation of the wave power. A number of mechanisms have been proposed to explain the acceleration of thermal electrons to relativistic energies, such as resonant interactions with monochromatic waves [Elkington et al., 1999], or statistical diffusion following interaction with a broadband spectrum [Liu et al., 1999]. Impulse responses of the energetic electron flux to the solar wind velocity have been calculated for fluxes at geosynchronous orbit [Baker et al., 1990] and all L shells in 1-11 [Vassiliadis et al., 2002; Rigler et al., 2004]. Over a region termed P_1, L=4-7.5, the flux begins to increase at τ=0 and reaches its maximum at τ=2 days. Therefore it is plausible that the wave power accumulated from τ=-2 days to τ=0 is at least in part provided to low-energy electrons (10-100 keV) which are accelerated to relativistic energies. ULF waves are involved in various types of mechanisms, depending on location, spectral characteristics, energy, and pitch angle. However, the observed energy densities of energetic electrons are not sufficiently high to account for the damping of the entire wave power.

Plasmaspheric electrons are another possible energy sink. As ULF waves propagate to plasmaspheric and ionospheric heights, they are partially reflected and absorbed [Takahashi et al., 1992]. Electromagnetic ion cyclotron (EMIC) waves are Landau-damped and contribute to the heating of thermal plasmaspheric electrons. Cornwall et al. [1971] estimated the energy absorbed by electrons through Landau damping of these ion cyclotron waves. Together with energy deposition from Coulomb interactions with ring current ions, they found that the combined heat flux to the ionosphere is sufficient to drive the stable aurora red (SAR) arcs to observable intensities. A more detailed calculation of the EMIC wave energy transfer to the thermal plasmas due to Landau damping was made by Gorbachev et al. [1992]: the heat flux to electrons is ~3×10^{10} eV $cm^{-2}sec^{-1}$, compared to ~4×10^{8} eV $cm^{-2}sec^{-1}$ for ions. The plasmasphere temperatures calculated including this heat source agree with spacecraft observations. Thus EMIC waves are the intermediaries for the transfer of energy from solar wind flows to plasmaspheric and other magnetospheric plasmas [Fok et al., 2005]. The former provide the free energy for wave generation while the latter are heated by the wave damping.

A third channel for dissipating the wave energy occurs during substorms. ULF waves are damped when increases in the ionospheric conductance lead to rapid dissipation of the stored energy. Ionospheric electron populations can be accelerated and heated as a result.

6. Summary

In the interaction between solar wind and inner magnetosphere including radiation belts and plasmasphere, ULF waves are an important part of the energy transfer. We have examined the time variations of ground and geosynchronous-orbit ULF wave power as a function of the solar wind velocity. We used both regular and rank-order correlation analysis to show that waves begin and end before the solar wind velocity reaches a peak value. The decline of the wave power before the solar wind velocity peak indicates that damping processes such as wave particle interaction can overcome the excitation by the still increasing solar wind velocity. In addition, we have obtained an FIR model which reproduces the response of the wave power to P_{ULF}. The rapid decrease of the wave power is in part due to the dV_{SW}/dt effect (loss of driver) and in part due to acceleration of cold electrons and ring current ions (availability of energy sinks). We have seen that the growth and decay patterns are characteristic for all L shells greater than 4. By examining the spatial responses at higher resolution than earlier studies, we have found a high degree of simultaneous wave activity over this region. However, it is clear that the response is more uniform at L shells beyond geosynchronous orbit compared to the region $4<L<6.6$ where the L profile of the wave power (and its response) are more structured and noisy. In contrast to these two regions, magnetometers at lower L shells, L=3.5-4, show a low wave power and a low-amplitude correlation and response, except at times of highly disturbed activity and ULF wave penetration in those L shells.

The partitioning of the L range in three different regions according to time variations of the ULF wave activity shares several features with the electron-radiation-belt regions identified from the time variations of the relativistic electron flux [Vassiliadis et al., 2002; 2003]. The ULF wave power profile is most probably related to the effects of the waves on the acceleration of thermal electrons to relativistic energies. Identifying the relative significance of various energy pathways (cold/thermal electrons; ring current ions; etc.) is an important challenge for future missions such as ORBITALS and RBSP. Modeling and analysis of past and existing missions can therefore provide valuable information for maximizing return from these future projects.

Acknowledgements. We thank the staff of the Finnish Meteorological Institute, especially A. Pulkkinen and A. Viljanen, for providing the IMAGE data. Interplanetary and magnetospheric data

were provided by NASA/NSSDC, NOAA/NGDC, and the Kyoto World Data Center. We thank M.-C. Fok and N. Tsyganenko for discussions. This research was supported by National Science Foundation grant 0418857 and NASA grant NAG5-12431, and CISM contract 47.050.

References

Anderson, B.J., M.J. Engebretson, and S.P. Rounds, A statistical study of Pc 3-5 pulsations observed by the AMPTE/CCE magnetic fields experiment 1. Occurrence distributions, J. Geophys. Res. 95, A7, 10,495-10,523, 1990.

Baker, D. N., R. L. McPherron, T. E. Cayton, R. W. Klebesadel, Linear prediction filter analysis of relativistic electron properties at 6.6 RE, J. Geophys. Res. 95, A9, 15,133-15,140, 1990.

Bargatze, L.F., D.N. Baker, R.L. McPherron, and E.W. Hones, Jr., Magnetospheric impulse response for many levels of geomagnetic activity, J. Geophys. Res. 90, A7, 6,387-6,394, 1985.

Clauer, C.R., The technique of linear prediction filters applied to studies of solar wind-magnetosphere coupling, in: Solar Wind-Magnetosphere Coupling, Y. Kamide and J.A. Slavin (eds.), 39-57, Terra Scientific, 1986.

Cornwall, J.M., F.V. Coroniti, and R.M. Thorne, Unified theory of SAR arc formation at plasmapause, J. Geophys. Res. 76, 19, 4428, 1971.

Elkington, S.R., M.K. Hudson, A.A. Chan, Acceleration of relativistic electrons via drift-resonant interaction with toroidal-mode Pc5 ULF oscillations, Geophys. Res. Lett. 26, 21, 3273-3276, 1999.

Engebretson, M., K. Takahashi, and M. Scholer, *Solar Wind Sources of Magnetospheric Ultra-Low Frequency Waves*, American Geophysical Union, Washington, DC, 1994.

Engebretson, M., K.-H. Glassmeier, M. Stellmacher, W.J. Hughes, H. Luehr, The dependence of high-latitude Pc5 wave power on solar wind velocity and on the phase of high-speed solar wind streams, J. Geophys. Res. 103, A11, 26,271-26,283, 1998.

Farrugia, C.J., F.T. Gratton, R.B. Torbert, Viscous-type processes in the solar wind-magnetosphere interaction, Space Sci. Rev. 95, 1-2, 443-456, 2001.

Fok, M.-C., Y. Ebihara, and T.E. Moore, Inner magnetospheric plasma interactions and coupling with the ionosphere, Adv. Pol. Upper Atm. Res. 19, 106-134, 2005.

Gonzalez, W.D., B.T. Tsurutani, and A.L.C. De Gonzalez, Interplanetary origin of geomagnetic storms, Space Sci. Rev. 88, 3-4, 529-562, 1999.

Gorbachev, O.A., G.V. Khazanov, K.V. Gamayunov, and E.N. Krivorutsky, A theoretical model for the ring current interaction with the Earth's plasmasphere, Planet. Space Sci., 40, 6, 859-872, 1992.

Gustafsson, G., N. E. Papitashvili, and V. O. Papitashvili, A Revised Corrected Geomagnetic Coordinate System for Epochs 1985 and 1990, *J. Atmos. Terr. Phys.*, 54, 1609-1631, 1992.

Hudson, M.K., S.R. Elkington, J.G. Lyon, C.C. Goodrich, T.J. Rosenberg, Simulation of radiation belt dynamics driven by solar wind variations, 171-182, in: *Sun-Earth Plasma Connections*, J.L. Burch, R.L. Carovillano, and S.K. Antiochos (eds.), Geophysical Monograph 109, American Geophysical Union, Washington, DC, 1999.

Lanzerotti, L.J., H.P. Lie, and N.A. Tartagli, Conjugate geomagnetic studies near the plasmapause, Antarct. J. US 6, 4, 129, 1971.

Liu, W.W., G. Rostoker, and D. N. Baker, Internal acceleration of relativistic electrons by large-amplitude ULF pulsations, J. Geophys. Res. 104, A8, 17,391-17,407, 1999.

Mann, I.R., A.N. Wright, K.J. Mills, and V.M. Nakariakov, Excitation of magnetospheric waveguide modes by magnetosheath flows, J. Geophys. Res. 104, A1, 333-353, 1999.

Mann, I.R., T.P. O'Brien, and D.K. Milling, Correlations between ULF wave power,solar wind speed, and relativistic electron flux in the magnetosphere: solar cycle dependence, J. Atm. Sol.-Terr. Phys. 66, 187-198, 2004.

Posch, J.L., M.J. Engebretson, V.A. Pilipenko, W.J. Hughes, C.T. Russell, L.J. Lanzerotti, Characterizing the long-period ULF response to magnetic storms, J. Geophys. Res. 108, A1, 1029, doi: 10.1029/2002JA009386, 2003.

Rigler, E.J., D.N. Baker, R.S. Weigel, D. Vassiliadis, and A.J. Klimas, Adaptive linear prediction of radiation belt electrons using the Kalman filter, Space Weather 2, 3, 2004.

Rostoker, G., S. Skone, and D.N. Baker, On the origin of relativistic electrons in the magnetosphere, Geophys. Res. Lett. 25, 3701-3704, 1998.

Takahashi, K., and B.J. Anderson, Distribution of ULF energy (f<80 mHz) in the inner magnetosphere – A statistical analysis of AMPTE CCE magnetic-field data, J. Geophys. Res. 97, A7, 10751-10773, 1992.

Takahashi, K., R.E. Denton, R.R. Anderson, and W.J. Hughes, Frequencies of standing Alfven wave harmonics and their implication for plasma mass distribution along geomagnetic field lines: Statistical analysis of CRRES data, J. Geophys. Res. 109, A8, Art. No. A08202, 2004.

Thorne, R.M., and R.B. Horne, Energy transfer between energetic ring current H+ and O+ by electromagnetic ion-cyclotron waves, J. Geophys. Res. 99, A9, 17275-17,282, 1994.

Vassiliadis, D., A. J. Klimas, S. G. Kanekal, D. N. Baker, R. S. Weigel, Long-term average, solar-cycle, and seasonal response of magnetospheric energetic electrons to the solar wind speed, *J. Geophys. Res.*, 10.1029/2001JA000506, 2002.

Vassiliadis, D., R.S. Weigel, A.J. Klimas, S.G. Kanekal, R.A. Mewaldt, Modes of energy transfer between the solar wind and the inner magnetosphere, Phys. Plasmas **10** (2), 463-473, 2003.

Vassiliadis, D., S.F. Fung, and A.J. Klimas, Solar, interplanetary and magnetospheric state parameters for the radiation belt electron flux, J. Geophys. Res. 110, A4, Art. No. A04201, 2005.

Wright, A.N., and G.J. Rickard, A numerical study of resonant absorption in a magnetohydrodynamic cavity driven by a broad-band spectrum, Astroph. J. 444, 1, 458-470, 1995.

Figure Captions

1. Stack plot of daily-averaged square root of the Pc3-Pc5 wave power, $P_{ULF}^{1/2}$ for 25 stations of the IMAGE array arranged from geomagnetic North (top) to South (bottom). The large excursions at DOY 300-304 were recorded during the "Halloween" storms at the end of October/beginning of November 2003.

2. Top: hourly averages of P_{ULF} at Tromso (L=6.36) in January 2003. Bottom: Simultaneous solar wind velocity from OMNI.

3. Correlation function (Eq. (1)) between the ground ULF wave power and solar wind velocity, for measurements made at the ground stations of Tromso (TRO) and Oulujaervi (OUJ), and at geosynchronous orbit (GOES-10). The time lag is measured in reference to the solar wind velocity.

4. As in Fig. 3, but for rank-order correlation functions and an hourly time resolution.

5. Rank-order correlation functions (see Fig. 4) have been interpolated in L to produce a two-argument (τ, L) function. The left graph is based on daily averages spanning 2002 and the right spanning 2003.

6. Impulse response function (Eq. (3)) of the ground ULF wave power to the solar wind velocity, for measurements made at TRO, OUJ, and at geosynchronous orbit (GOES-10). The time lag is measured with reference to the solar wind velocity.

7. As in Fig. 6, but for the rank-order impulse response function.

8. Rank-order impulse response functions (see Fig. 7) have been interpolated in L to produce a two-argument (τ, L) function calculated for all data (2002-2003). Diamonds on the left side of the graph indicate the locations of individual ground stations.

9. a. The impulse response function at zero lag, $H_{V_{sw}}^{ULF}(0,L)$ as a function of L shell. Regions can be identified based on the coupling strength and are marked by vertical dotted lines. b. Data-model correlation coefficient, both regular (black) and rank-ordered (green) P_{ULF} data, as a function of L shell. For reference, the horizontal dotted line indicates a correlation coefficient of 70% corresponding to a prediction efficiency value of ~50%.

FIGURE 1

TIME VARIATIONS OF ULF WAVE POWER:
IMAGE MAG ARRAY, 2003

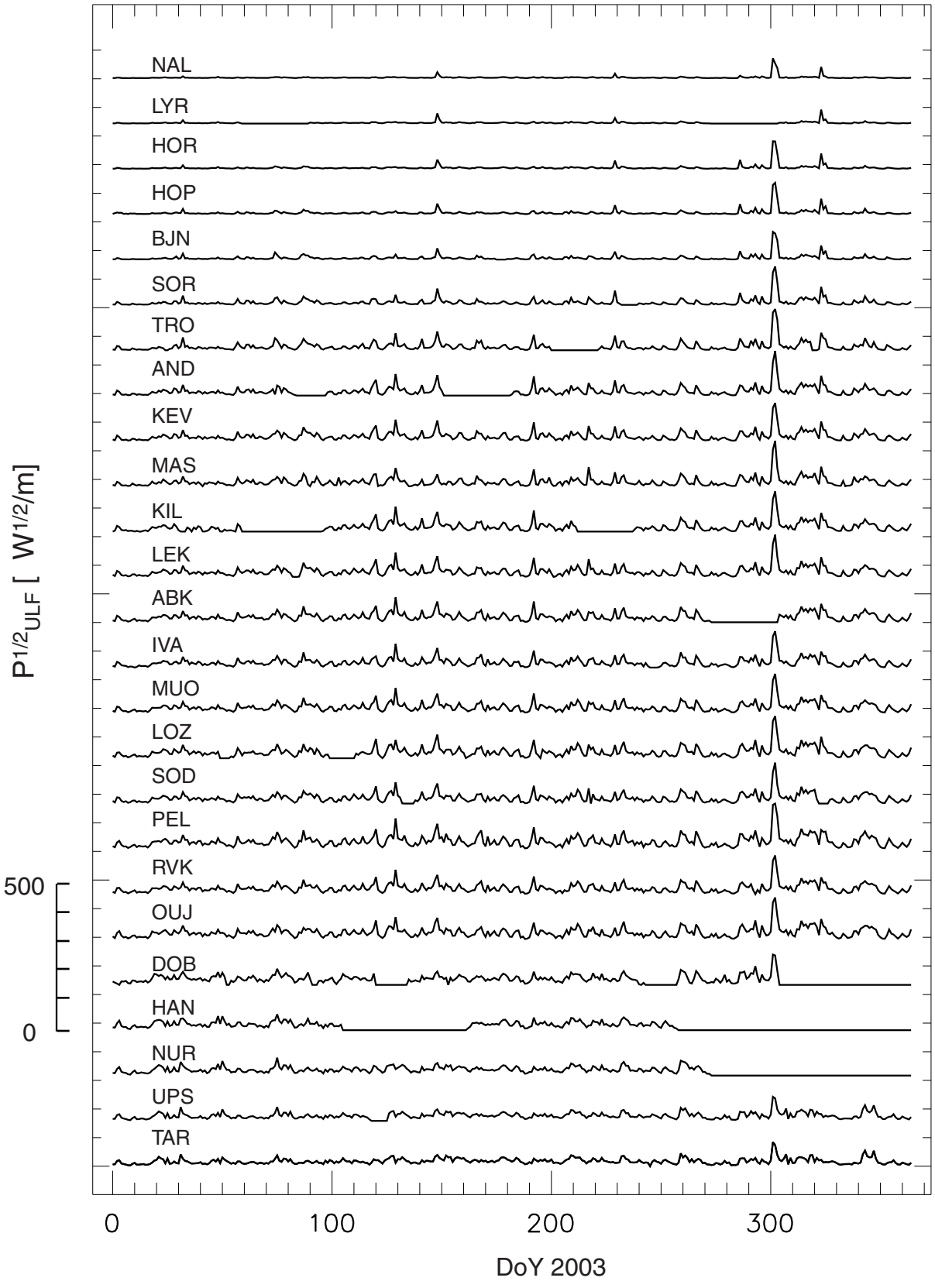

FIGURE 2

ULF POWER AND SOLAR WIND VELOCITY:
January 1-28, 2003

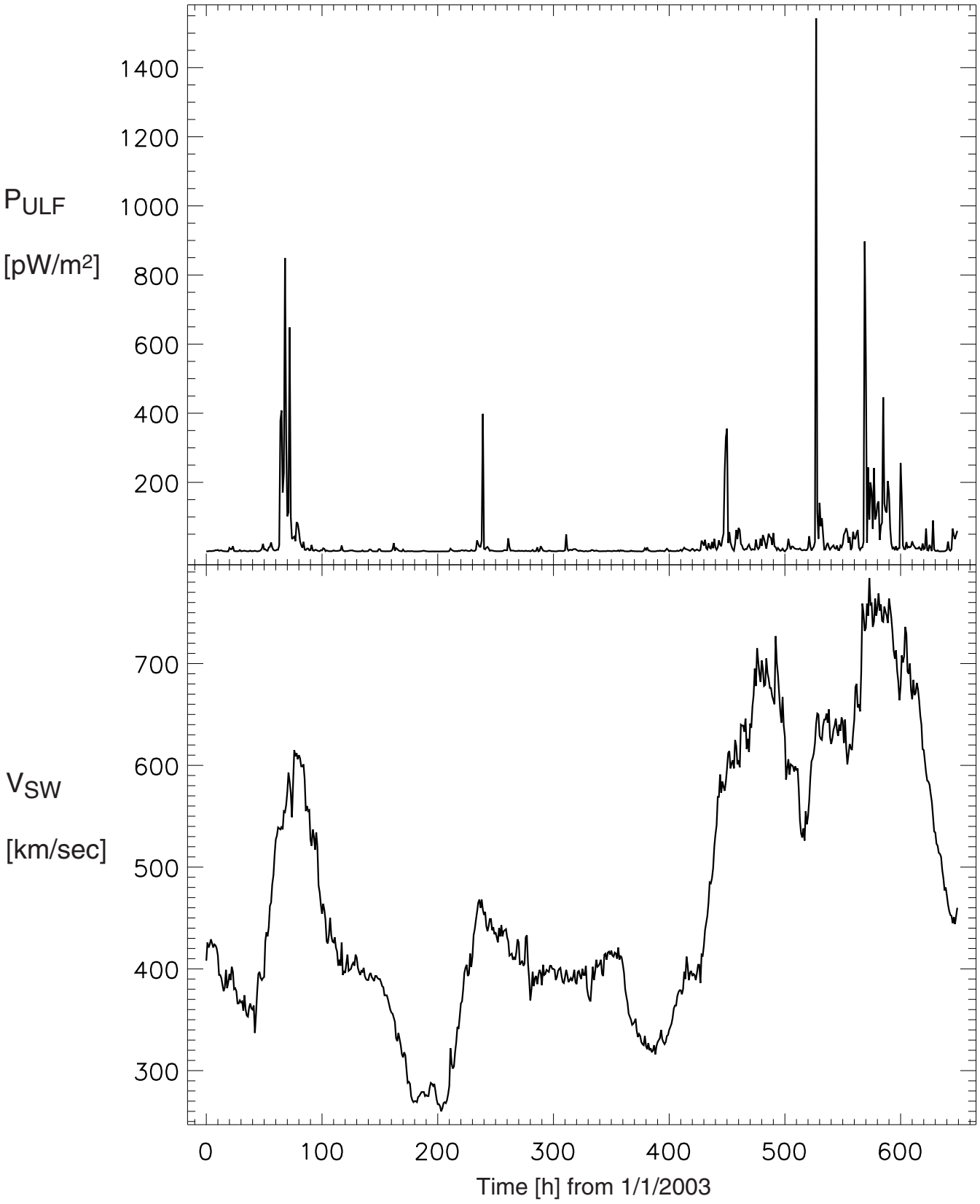

FIGURE 3

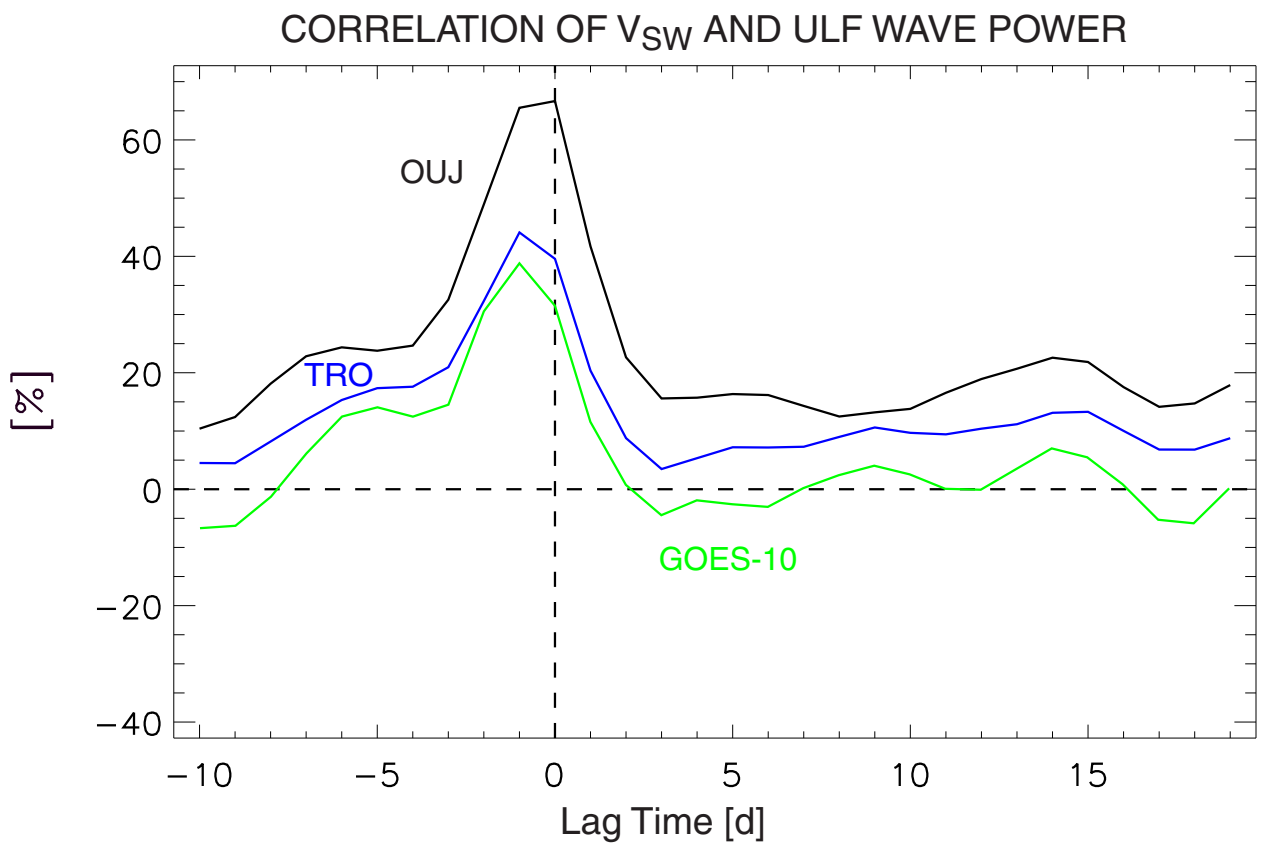
CORRELATION OF V_{SW} AND ULF WAVE POWER
60
40
20
0
−20
−40
[%]
OUJ
TRO
GOES-10
−10
−5
0
5
10
15
Lag Time [d]

FIGURE 4

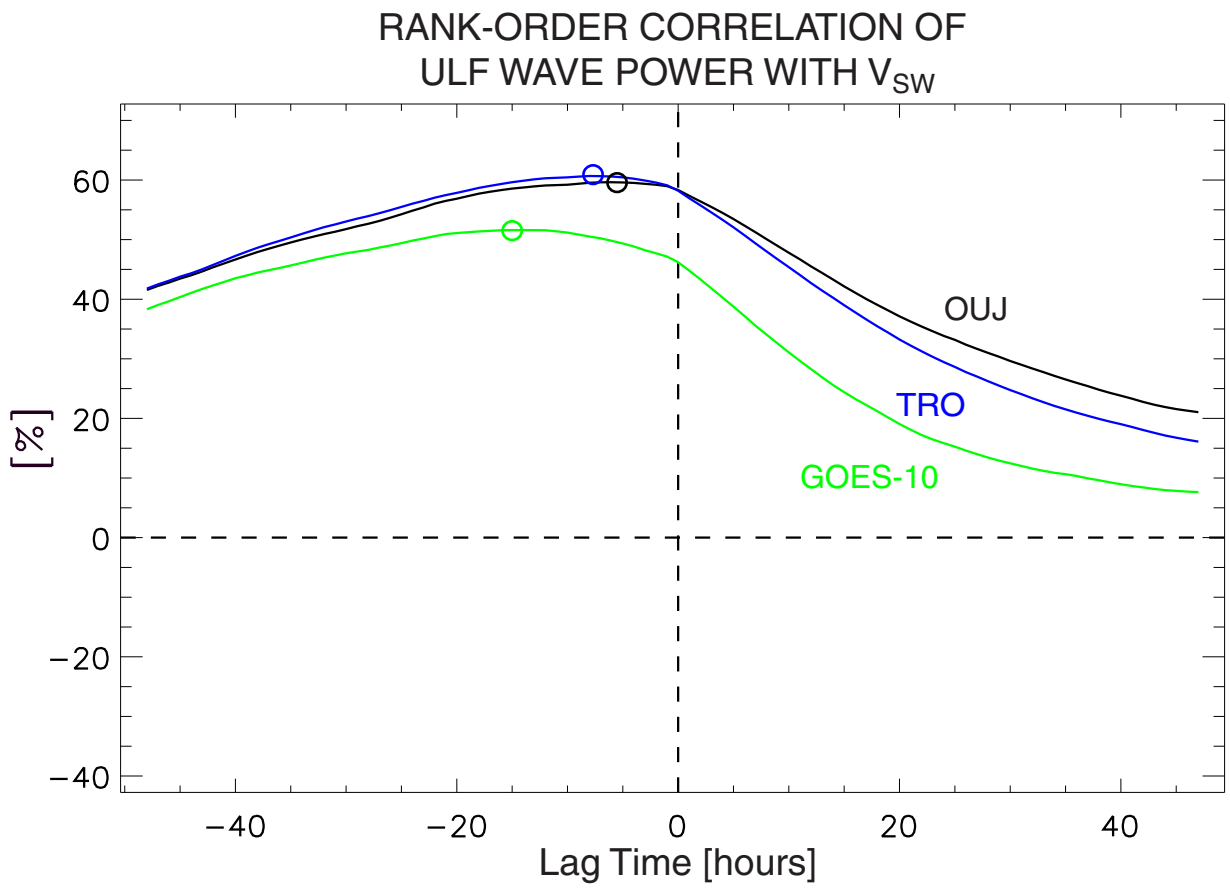
RANK-ORDER CORRELATION OF
ULF WAVE POWER WITH V_{SW}
60
40
20
0
−20
−40
[%]
−40
−20
0
20
40
Lag Time [hours]
OUJ
TRO
GOES-10

FIGURE 5

RANK-ORDER CORRELATION FUNCTION
OF P_{ULF} WITH V_{SW}

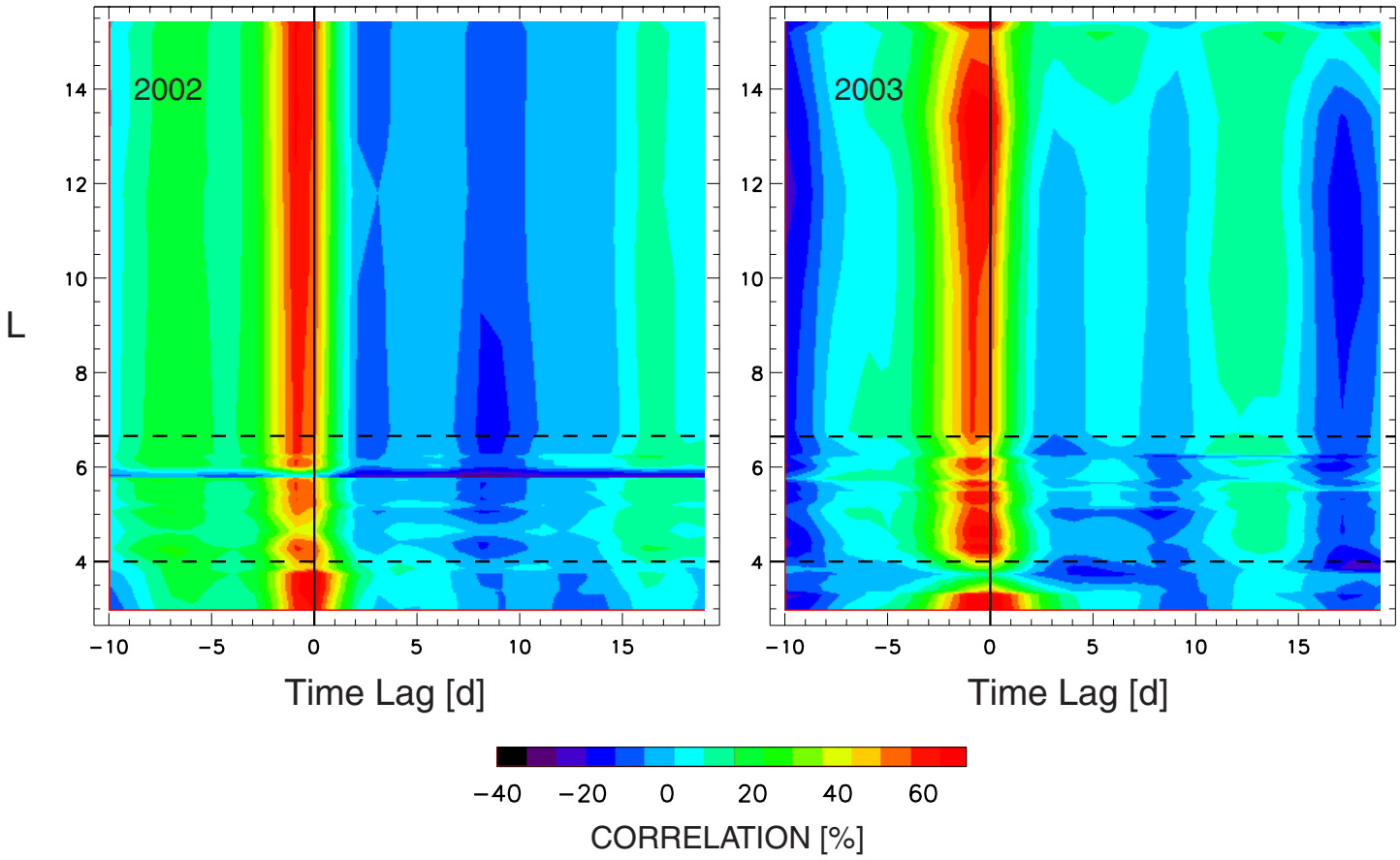

FIGURE 6

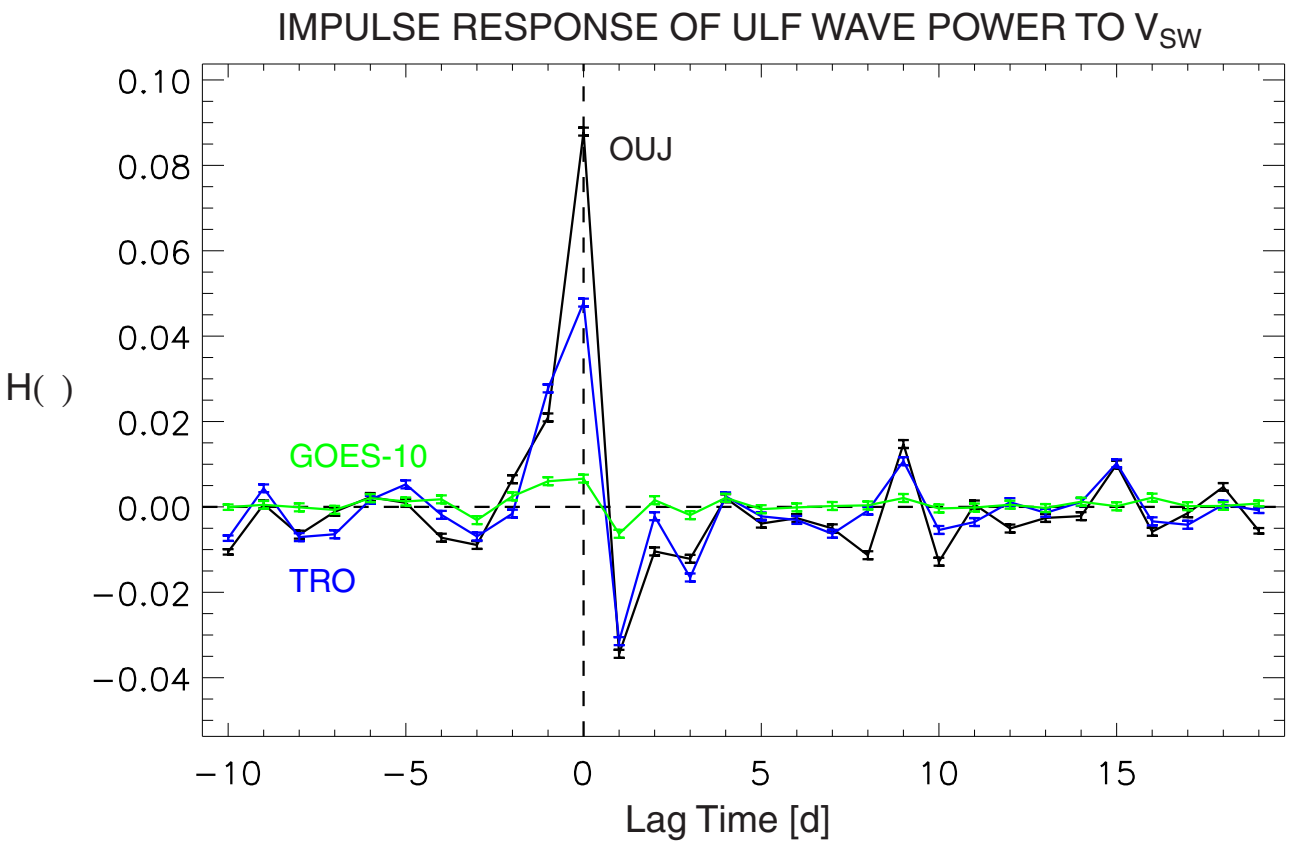
IMPULSE RESPONSE OF ULF WAVE POWER TO V_{SW}
H( )
0.10
0.08
0.06
0.04
0.02
0.00
−0.02
−0.04
OUJ
GOES-10
TRO
−10
−5
0
5
10
15
Lag Time [d]

FIGURE 7

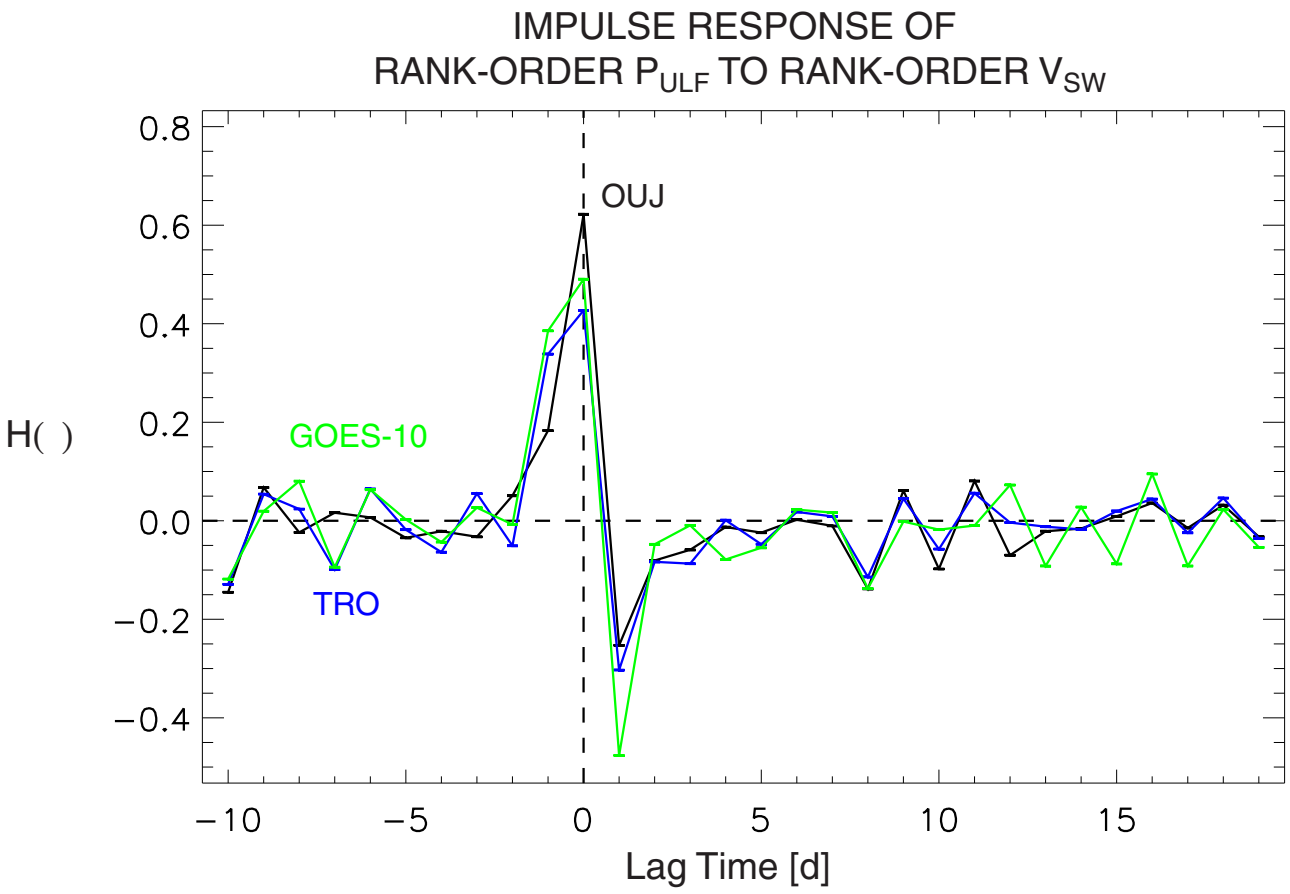
IMPULSE RESPONSE OF
RANK-ORDER P_{ULF} TO RANK-ORDER V_{SW}
H( )
0.8
0.6
0.4
0.2
0.0
−0.2
−0.4
OUJ
GOES-10
TRO
−10
−5
0
5
10
15
Lag Time [d]

FIGURE 8

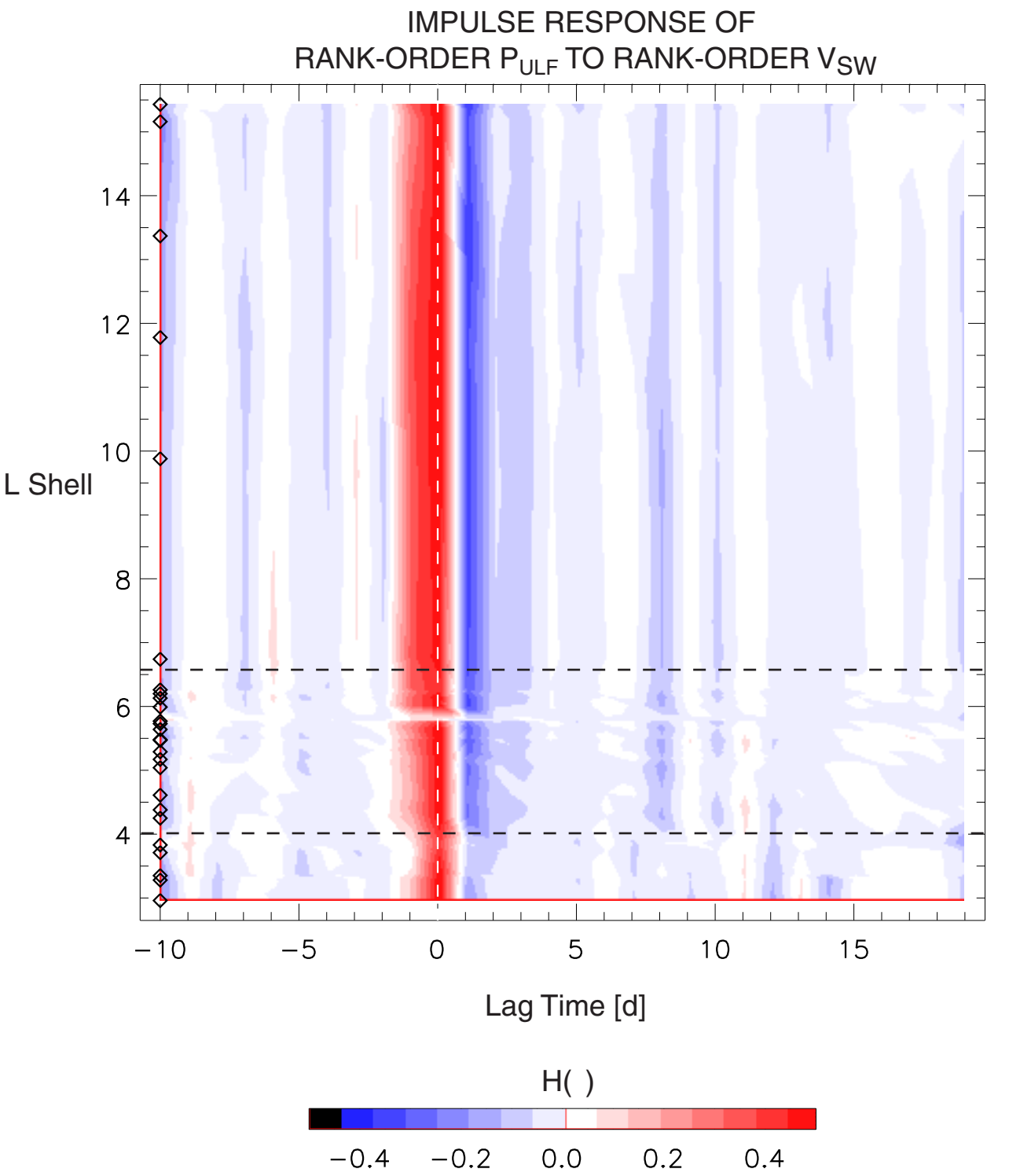
IMPULSE RESPONSE OF
RANK-ORDER P_{ULF} TO RANK-ORDER V_{SW}
L Shell
14
12
10
8
6
4
−10
−5
0
5
10
15
Lag Time [d]
H( )
−0.4
−0.2
0.0
0.2
0.4

FIGURE 9

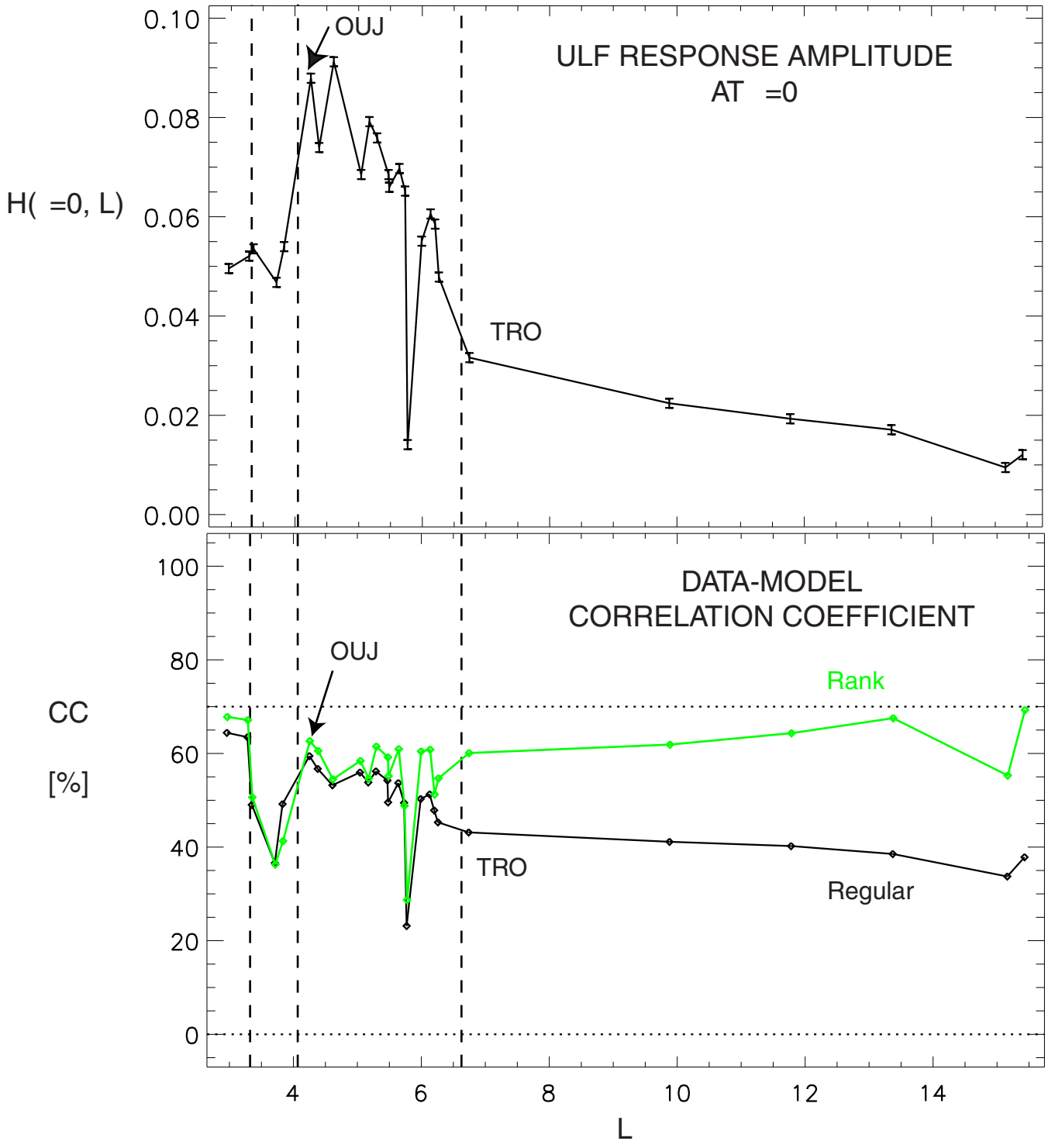
ULF RESPONSE AMPLITUDE
AT =0
H(=0, L)
0.10
0.08
0.06
0.04
0.02
0.00
OUJ
TRO
DATA-MODEL
CORRELATION COEFFICIENT
CC
[%]
100
80
60
40
20
0
Rank
Regular
4
6
8
10
12
14
L